A numerical solution to seepage problems with complex drainage systems

Yifeng Chen [a,*], Chuangbing Zhou [a], Hong Zheng [b]

[a] *State Key Laboratory of Water Resources and Hydropower Engineering Science, Wuhan University, Wuhan 430072, China*
[b] *Institute of Rock and Soil Mechanics, Chinese Academy of Sciences, Wuhan 430071, China*

Abstract

Seepage problems with complex drainage systems are commonly encountered in civil engineering, with strong non-linearity. A numerical solution based on the Finite Element Method combining the substructure technique with a variational inequality formulation of Signorini's type is proposed to solve these problems. The aims of this work are to accurately characterize the boundary conditions of the drainage systems, to reduce the difficulty in mesh generation resulting from the drainage holes with small radius and dense spacing, and to eliminate the singularity at the seepage points and the resultant mesh dependency. Numerical stability and robustness of the proposed method are guaranteed by an adaptive procedure for progressively relaxing the penalized Heaviside function associated with the formulation of the discrete variational inequality. Two challenging numerical examples are presented to validate the effectiveness and robustness of the proposed method.
© 2007 Elsevier Ltd. All rights reserved.

Keywords: Seepage problem; Drainage system; Substructure technique; Variational inequality; Adaptive penalized Heaviside function

1. Introduction

In dam engineering, slope engineering and underground engineering etc., the deformation and stability of geotechnical structures are significantly influenced by the seepage flow within them. In order to control the seepage flow and to eliminate its unfortunate effects, a complex drainage system including drainage galleries, drainage tunnels, draining wells and drainage hole arrays is commonly designed and deployed. For the purposes of safety assessment and optimization design of the drainage system, numerical analysis has to be performed.

Although significant achievement has been made in the analysis of seepage flow with the finite element method, modeling the seepage problem with a complex drainage system remains a challenging problem. Such a problem usually involves two sources of difficulty: the first difficulty relates to the FE mesh generation with hundreds or even thousands of drainage holes with small diameter and dense spacing, while the other difficulty relates to the strong non-linearity in the determination of the free surface. To avoid the first difficulty, both the explicit method and the implicit method are used. The explicit method [1] models the drainage hole curtain with an equivalent medium which may produce the same flow rate. The implicit method models the drainage hole array with a substructure technique [2,3], a semi-analytical approach [4,5], a point well model [6], or a composite element method [7]. Most of the existing models (except the substructure technique), however, fail more or less to precisely describe the details of the boundary conditions of the drainage facilities, and thus, sacrifice to some degree the theoretical strictness of solutions.

In addition to adaptive mesh methods, two categories of fixed mesh methods, i.e. the intuitive methods and the variational inequality methods, are widely used to determine the free surface and the seepage points. In the literature, the residual flow method [8], the initial flow method [9],

---
* Corresponding author. Tel.: +86 27 68772221; fax: +86 27 68772310.
E-mail address: csyfchen@whu.edu.cn (Y. Chen).

and the adjusting permeability method [10] etc., fall into the intuitive methods, and they usually involve an iterative procedure to ensure that the flow in the dry domain is much lower than that in the wet domain. With the support of a rigorous mathematical theory, on the other hand, the variational inequality methods always transform the free surface and its condition to an inner boundary condition by defining a new boundary value problem on a fixed domain. Before Zheng et al. [11] proposed the formulation of Signorini's type, the existing variational inequality methods, including an expanded pressure formulation by Brezis et al. [12], did not theoretically overcome the singularity at the seepage points and thus led to an undesirable mesh dependency.

For solving seepage problems with a complex drainage system, the drainage galleries or tunnels with relatively large sizes and regular shapes and extensions can generally be explicitly modeled in the FEM and be properly addressed as long as their boundary conditions are properly prescribed. Special attention, however, has to be given to the large number of drainage holes. In this study, a substructure technique has been developed to model the effects of a drainage hole array, with a capability in simplifying the generation of a FE mesh and characterizing the boundary conditions of the drainage holes. This technique was initially developed by Wang et al. [2] for modeling the drainage holes not intersecting the free surfaces, and later improved by Zhu and Zhang [3] in combination with the initial flow method for modeling drainage holes intersecting with any free surfaces. The presence of drainage holes produces singular seepage points, and due to the reasons described earlier, the accuracy of the above solution may be unsatisfactory with numerical fluctuations in results.

In this study, we address the seepage problems with complex drainage systems using a method combining the substructure technique with the variational inequality formulation of Signorini's type by Zheng et al. [11]. An adaptive procedure is proposed to guarantee numerical stability and robustness of the proposed method, through progressively relaxing the penalized Heaviside function associated with the formulation of the discrete variational inequality. The remainder of this paper is arranged as follows: Section 2 describes seepage problems with free surfaces based on the variational inequality formulation of Signorini's type. In Section 3, the boundary conditions of such drainage systems are summarized, the substructure method is introduced to model the drainage hole array, and a numerical algorithm is presented to address seepage problems with drainage systems. In Section 4, two challenging numerical examples are given to demonstrate the effectiveness of the proposed method, which is followed by concluding remarks presented in Section 5.

2. Formulation of seepage problems with free surfaces [11]

As shown in Fig. 1, the seepage flow through domain Ω is actually the flow through the wet domain Ω_w below the
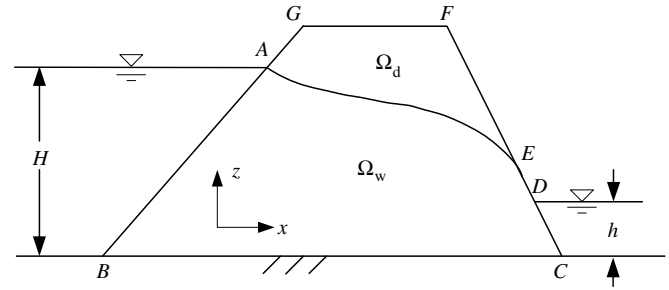

Fig. 1. Illustration of seepage flow through a soil dam (after [11]).

free surface Γ_f. The wet domain Ω_w will be determined as long as the free surface Γ_f is located, which, in many engineering cases is unknown in advance. To define a new boundary value problem on the entire domain Ω, as a variational inequality formulation requires, Darcy's law is redefined as follows:

$$\boldsymbol{v} = -\boldsymbol{k}\nabla\phi + \boldsymbol{v}_0 \tag{1}$$

where $\boldsymbol{v}$ is the flow velocity, $\boldsymbol{v}_0$ the initial flow velocity, $\boldsymbol{k}$ the second-order hydraulic conductivity tensor, ∇ the gradient operator, $\phi = z + p/\gamma_w$ the total water head, z the vertical coordinate, p the pore water pressure, γ_w the unit weight of water. Here, $\boldsymbol{v}_0$ is introduced to eliminate the virtual flow velocity on the dry domain Ω_d, in the form of

$$\boldsymbol{v}_0 = H(\phi - z)\boldsymbol{k}\nabla\phi \tag{2}$$

in which $H(\phi - z)$ is a Heaviside function

$$H(\phi - z) = \begin{cases} 0 & \text{if } \phi \geqslant z \ (\text{in } \Omega_w) \\ 1 & \text{if } \phi < z \ (\text{in } \Omega_d) \end{cases} \tag{3}$$

The seepage flow through domain Ω ($\Omega = \Omega_w \cup \Omega_d$) is then governed by the following equation of continuity:

$$\nabla \cdot \boldsymbol{v} = 0 \ (\text{in } \Omega) \tag{4}$$

subjected to the following boundary conditions:

(1) The water head boundary condition

$$\phi = \bar{\phi} \ (\text{on } \Gamma_\phi = \text{AB} + \text{CD}) \tag{5}$$

in which $\bar{\phi}$ is the prescribed water head on Γ_ϕ.
(2) The flux boundary condition

$$q_n \equiv -\boldsymbol{n}^\mathrm{T}\boldsymbol{v} = \bar{q}(\text{on } \Gamma_q = \text{BC}) \tag{6}$$

where $\bar{q}$ is the prescribed flux on Γ_q, $\boldsymbol{n}$ the outward unit normal vector to the boundary. For an impermeable boundary, $\bar{q} = 0$.
(3) The boundary condition of Signorini's type on the seepage surface

$$\begin{cases} \phi \leqslant z, & q_n(\phi) \leqslant 0 \\ (\phi - z)q_n(\phi) = 0 \end{cases} \quad (\text{on } \Gamma_s = \text{DEFGA}) \tag{7}$$

in which Γ_s is the potential seepage boundary. Obviously, on section DE, $\phi = z$ and $q_n \leqslant 0$; while on section EFGA, $\phi < z$ and $q_n = 0$. $\phi = z$ and $q_n = 0$ are satisfied at the seepage point E.

(4) The boundary condition on the free surface

$$q_n|_{\Omega_w} = q_n|_{\Omega_d} = 0 \quad (\text{on } \Gamma_f = \text{AE}) \tag{8}$$

in which $\Gamma_f \equiv \{(x, y, z) | \phi = z\}$ is the free surface, an interface between Ω_w and Ω_d.

Based on the above PDE formulation, Zheng et al. [11] developed an equivalent variational inequality formulation for the problem. The mathematical statement for a discrete version of the iterative formulation is given as: Find a vector $\phi^{k+1} \in \Phi_{VI}^h$, such that for $\forall \psi \in \Phi_{VI}^h$, the following inequality holds:

$$(\psi - \phi^{k+1})^T K \phi^{k+1} \geqslant (\psi - \phi^{k+1})^T q^k \tag{9}$$

with

$$K = \sum_e k^e, \quad k^e = \int\int\int_{\Omega_e} B^T k B \, d\Omega \tag{10}$$

$$q^k = \sum_e \int\int\int_{\Omega_e} B^T v_0^k \, d\Omega = K_\varepsilon \phi^k, \quad K_\varepsilon = \sum_e k_\varepsilon^e,$$

$$k_\varepsilon^e = \sum_e \int\int\int_{\Omega_e} H_\lambda(\phi^k - z) B^T k B \, d\Omega \tag{11}$$

$$\Phi_{VI}^h = \{\phi | \phi \in R^n; \phi_i = \bar{\phi}_i, \text{ for } i \in \Gamma_\phi; \phi_i \leqslant z_i, \text{ for } i \in \Gamma_s\} \tag{12}$$

where k is the iterative step, n the total number of nodal points in the FE mesh, B the geometrical matrix of the finite element model, and H_λ the penalized Heaviside function introduced to evade numerical instability and mesh dependency, given by

$$H_\lambda(\phi - z) = \begin{cases} 1 & \text{if } \phi \leqslant z - \lambda_1 \\ \frac{z + \lambda_2 - \phi}{\lambda_1 + \lambda_2} & \text{if } z - \lambda_1 < \phi < z + \lambda_2 \\ 0 & \text{if } \phi \geqslant z + \lambda_2 \end{cases} \tag{13}$$

in which λ_1 and λ_2 are two parameters associated with each element. The parameter λ_1 is defined as the vertical distance between the lowest integration point to the lowest node, and λ_2 as the vertical distance between the highest integration point to the highest node, in the FEM model concerned.

It is to be noted that in Eq. (11), the flux boundaries are assumed to be impermeable. If non-zero flux boundaries are involved, their contribution has to be added to the right hand vector, q^k.

Without losing generality, the nodal set N may be divided into the following three subsets:

$$N_\phi = \{i \in N | i \in \Gamma_\phi\}, \quad N_s = \{i \in N | i \in \Gamma_s\},$$
$$N_i = N - N_\phi - N_s$$

Eq. (9) can then be solved by the following two steps of iteration:

Step 1: solve $\sum_j K_{ij} \phi_j^{k+1} - q_i^k = 0$, for $\forall i \in N_i$.
Step 2: solve $(\phi_i^{k+1} - z_i) \theta_i^{k+1} = 0$, for $\forall i \in N_s$, where $\theta_i^{k+1} = \sum_j K_{ij} \phi_j^{k+1} - q_i^k$. With the algorithm proposed by Zheng et al. [13], usually a precise solution of Step 2 can be achieved in a very few iterations.

3. A substructure method for drainage hole array

In this section, we first characterize the possible boundary conditions of the drainage facilities, and then a substructure method is presented to model densely-deployed drainage holes of small diameter.

3.1. Boundary conditions of drainage system

To assess the effects of the drainage system, the boundary conditions of the drainage facilities involved have to be properly represented in the numerical analysis. The possible boundary conditions of the drainage holes and draining wells are illustrated in Fig. 2.

The first type of boundary condition is the Signorini's type, such as the vertical drainage holes deployed between two horizontal drainage galleries in a dam, in which the drainage flow is always discharged into the lower drainage gallery. As shown in Fig. 2a, on section AB of the drainage hole, the boundary condition satisfies $\phi < z$ and $q_n = 0$, while on section BC, it satisfies $\phi = z$ and $q_n \leqslant 0$.
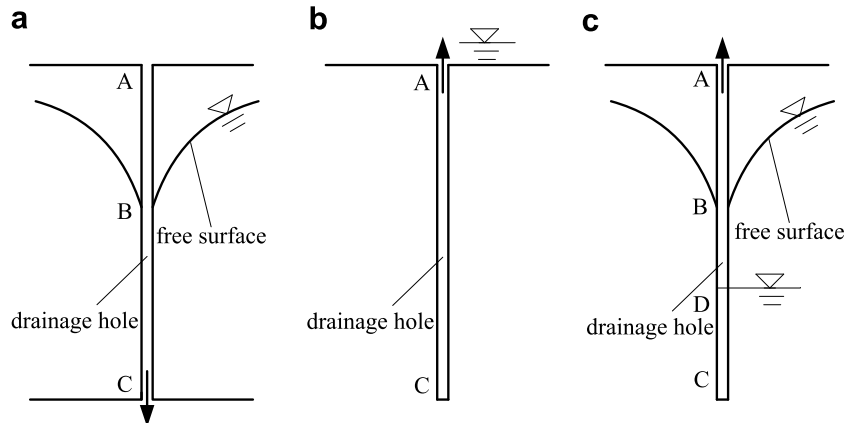

Fig. 2. Boundary conditions of drainage holes.

The second type is the water head boundary condition, as depicted in Fig. 2b. The drainage holes deployed in a rock foundation generally possess this type of boundary condition. The prescribed water head is usually determined by the floor elevation of the drainage gallery connected with the holes.

Associated with a draining well or a drainage hole in deficiency, the third type of boundary condition is actually a condition with known drainage flow rate out of the facility. As shown in Fig. 2c, part of the boundary, i.e. section AD, satisfies the complementary condition of Signorini's type, while the other part, i.e. section DC, satisfies the water head boundary condition (the 2nd type as defined above). The water head in the draining well or drainage hole is generally unknown *a priori*, and has to be determined by the flowrate, Q, through an iterative procedure as described below.

First, assume the whole boundary, i.e. section AC in Fig. 2c, to be a Signorini's type, and compute the drainage flow Q_c. In this circumstance, the computed drainage flow rate, Q_c, may exceeds the actual water yield, Q (i.e. $Q_c > Q$). Then, one needs to assign a proper counteracting increment of water head for the draining well or drainage hole according to the height of hydraulic jump and the ratio of Q/Q_c, and re-compute the value of Q_c. If the difference between Q and Q_c becomes smaller than a given tolerance, the procedure will be terminated. Otherwise, repeat the procedure by gradually increasing or decreasing the water head according to the magnitudes of Q and Q_c.

Compared with the drainage holes or draining wells, the boundary conditions of the drainage galleries or tunnels are easier to be identified. Generally, Signorini's type of boundary condition is satisfied on the boundaries of the galleries or tunnels. If, however, the drainage galleries or tunnels are submerged, then part or full of the boundary will satisfy the water head condition.

3.2. The substructure method

The basic idea of the substructure technique is to discretize the domain space disregarding the presence of drainage holes. The elements that contain one or multiple drainage holes are subdivided and the internal variables as well as the boundary properties of the drainage holes are eliminated, thus giving a considerable saving in the mesh-generating and equation-solving efforts.

Suppose that a drainage hole is embedded in a set of elements of eight nodes, as shown in Fig. 3. Each element is subdivided into two or three layers of sub-elements in the radial direction of the drainage hole, in which the circular cross section of the hole is replaced by a square one of the same perimeter length. As a result, a substructure is formed by all the sub-elements in the associated element set.

From the element faces to the boundaries of the drainage hole in the radial direction, three sets of nodes are identified: the outer set o, the median set m and the inner set i. The nodes in the outer set o are composed of the nodal
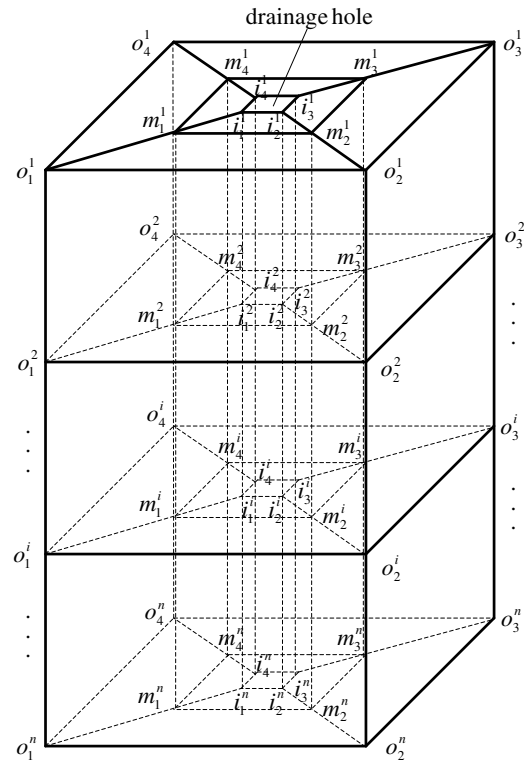

Fig. 3. Construction of a drainage substructure.

points on the associated elements, and are ordered from one end of the hole to the other, e.g. $o = \{o_1^1, o_2^1, o_3^1, o_4^1, \ldots, o_1^i, o_2^i, o_3^i, o_4^i, \ldots, o_1^n, o_2^n, o_3^n, o_4^n\}$ in Fig. 3. The nodes in the inner set i represent the boundary of the drainage hole, and their positions are determined by the location of the hole. The nodes in the median set m are interpolated between the nodes in set o and those in set i to ensure good shape of the sub-elements. If the original elements are large in size, then two or more layers of median nodes may be interpolated in order to create well shaped sub-elements. Note that the nodes in set i and set m are ordered in the same way as the nodes in set o.

In the formulation of the substructure algorithm, special consideration is required for the following two cases. First, if a drainage hole is vertically (or obliquely) deployed between two horizontal drainage galleries, as the case shown in Fig. 2a, the nodes in the median set m attached to the gallery surfaces share the same boundary conditions with the nodes in set i. These nodes should be removed from set m and added to set i. Second, if a drainage hole or a draining well is vertically (or obliquely) deployed in a rock foundation, as shown in Fig. 2b and c, the coarse element attached to the lower end of the hole or well should also be included in the substructure, but subdivided into several wedge-shaped sub-elements and a brick-shaped one, as depicted in Fig. 4. The problem with this scheme is that the sub-elements are poorly shaped and numerical difficulties may be caused. A better alternative, however, is to include all the elements intersected by the extending line of the drainage facility from the lower end in the
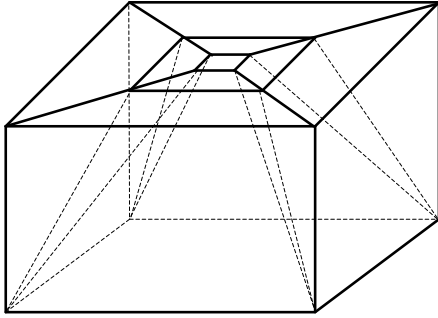
Fig. 4. A transition element at the end of a drainage substructure.

substructure to form a larger one. In this scheme, all the interpolated nodes (except those on the bottom of the hole) in these elements should be recorded in set $\boldsymbol{m}$. To save computational cost, these elements can also be arranged to form another substructure, but the nodes on the adjacent surface of the two substructures should be moved from set $\boldsymbol{m}$ to set $\boldsymbol{o}$.

From Section 3.1, it is clear that at the iterative step $k + 1$, one of the following two conditions should be satisfied for $\forall i \in \boldsymbol{i}$:

(1) $\phi_i = \bar{\phi}_i$ (the water head boundary condition), or
(2) $(\phi_i^{k+1} - z_i)\theta_i^{k+1} = 0$ with $\theta_i^{k+1} = \sum_{j \in i \cup m} K_{ij}\phi_j^{k+1} - q_i^k$ (the complementary condition of Signorini's type).

For the nodes in sets $\boldsymbol{o}$ and $\boldsymbol{m}$, the flow equilibrium equations at the iterative step $k+1$ are written as

$$\begin{bmatrix} \boldsymbol{K}_{oo} & \boldsymbol{K}_{om} \\ \boldsymbol{K}_{mo} & \boldsymbol{K}_{mm} \end{bmatrix} \left\{ \begin{array}{c} \boldsymbol{\phi}_o^{k+1} \\ \boldsymbol{\phi}_m^{k+1} \end{array} \right\} = \left\{ \begin{array}{c} \boldsymbol{q}_o^k - \boldsymbol{K}_{oi}\boldsymbol{\phi}_i^k \\ \boldsymbol{q}_m^k - \boldsymbol{K}_{mi}\boldsymbol{\phi}_i^k \end{array} \right\} \quad (14)$$

where $\boldsymbol{K}_{rs}$ is the stiffness sub-matrix between node set $\boldsymbol{r}$ and set $\boldsymbol{s}$ ($r, s = \boldsymbol{o}, \boldsymbol{m}, \boldsymbol{i}$), respectively, and $\boldsymbol{\phi}_r$ and $\boldsymbol{q}_r$ are the water head vector and the right hand side vector of the nodes in $\boldsymbol{r}$.

By eliminating the internal degrees of freedom, $\boldsymbol{\phi}_m^{k+1}$, Eq. (14) is rewritten as

$$\boldsymbol{K}_{oo}'\boldsymbol{\phi}_o^{k+1} = \boldsymbol{q}_o'^k \quad (15)$$

with

$$\boldsymbol{K}_{oo}' = \boldsymbol{K}_{oo} - \boldsymbol{K}_{om}\boldsymbol{K}_{mm}^{-1}\boldsymbol{K}_{mo} \quad (16)$$

$$\boldsymbol{q}_o'^k = \boldsymbol{q}_o^k - \boldsymbol{K}_{om}\boldsymbol{K}_{mm}^{-1}(\boldsymbol{q}_m^k - \boldsymbol{K}_{mi}\boldsymbol{\phi}_i^k) \quad (17)$$

After substitution of Eq. (15) into Eq. (14), $\boldsymbol{\phi}_m^{k+1}$ can be computed by

$$\boldsymbol{\phi}_m^{k+1} = \boldsymbol{K}_{mm}^{-1}(\boldsymbol{q}_m^k - \boldsymbol{K}_{mo}\boldsymbol{\phi}_o^{k+1} - \boldsymbol{K}_{mi}\boldsymbol{\phi}_i^k) \quad (18)$$

In Eq. (15), the condensed stiffness matrix, $\boldsymbol{K}_{oo}'$, can be determined by Eq. (16). The condensed right hand side vector, $\boldsymbol{q}_o'^k$, can also be determined by Eq. (17) because $\boldsymbol{q}_o^k$ and $\boldsymbol{q}_m^k$ can be computed by Eq. (11) over the relevant sub-elements, while $\boldsymbol{\phi}_i^k$ can be computed by the iterative procedure described in Section 2. It is easy to see that Eq. (14), and thus Eqs. (15) and (17) hold valid only if the whole element

set associated with the drainage hole is taken into account. If, however, only one of the elements is considered, the right hand side of Eq. (14) will become unknown.

The computational complexity of Eq. (15) is mainly determined by the inverse manipulation of the matrix, $\boldsymbol{K}_{mm}$. With the arrangement of the nodes in set $\boldsymbol{m}$, $\boldsymbol{K}_{mm}$ is a block tridiagonal symmetric matrix with block size of four for one layer of interpolated nodes and eight for two layers. As a result, the inverse of $\boldsymbol{K}_{mm}$ can be efficiently computed with the LDL$^\mathrm{T}$ decomposition of the block tridiagonal symmetric matrix [14]. Besides, in most of the practical engineering problems, the drainage holes are limited in length to, e.g. 15–30 m. Thus, not many elements will be associated with each of the drainage holes, resulting in small order and efficient inverse of $\boldsymbol{K}_{mm}$.

For practical purposes, especially for design optimization of drainage systems, the substructure can be used in a very flexible fashion [3], as shown in Fig. 5. As long as an additional computational cost can be afforded, multiple layers of linear sub-elements or high-order sub-elements can be inserted to form a substructure with improved accuracy. Also, multiple drainage holes densely deployed in one or even multiple rows can be embedded in substructure elements, although a considerable loss of accuracy may be incurred due to distorted element shapes and large element sizes.

3.3. Numerical implementation

The above substructure technique is implemented into a FEM code. First, for each drainage hole, find the elements intersecting with it and form the drainage substructures. The condensed stiffness matrices of the drainage substructures are computed by using Eq. (16) and assembled into the global stiffness matrix. Then, add the nodes on boundaries of the drainage holes (i.e. nodes in set $\boldsymbol{i}$ for each substructure) into N_s (see Section 2), call the procedure given
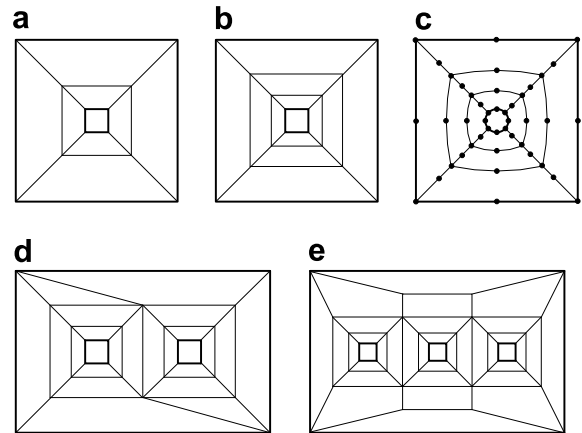

Fig. 5. Various forms of the drainage substructure: (a) one hole, two layers of sub-elements, consistent with Fig. 3; (b) one hole, three layers of sub-elements; (c) one hole, three layers of high-order sub-elements and (d) two holes, three layers of sub-elements; (e): three holes, three layers of sub-elements).

in Section 2 to determine the seepage points and to locate the seepage surface. If draining wells are involved in the problem, then an outer iterative procedure, as described in Section 3.1, has to be invoked to achieve the flow equilibrium of the draining wells.

The convergence criterion is defined as

$$\|\boldsymbol{\varphi}^{i+1} - \boldsymbol{\varphi}^i\|_1 < \varepsilon_1 \|\boldsymbol{\varphi}^i\|_1 \quad \text{and} \quad \|\boldsymbol{\varphi}^{i+1} - \boldsymbol{\varphi}^i\|_\infty < \varepsilon_2 \|\boldsymbol{\varphi}^i\|_\infty \tag{19}$$

in which ε_1 and ε_2 denote the user-specified error tolerances and take values of $\varepsilon_1 = 10^{-5}$ and $\varepsilon_2 = 10^{-3}$ in this study. According to the extremum principle of elliptical functions, ϕ reaches its maximum only on the boundary. Thus, it is obvious that $\|\phi\|_\infty$ is equal to the prescribed water head on the upstream surface.

The above algorithm can run rather efficiently in computation, since the global stiffness matrix remains constant during iterations and need only be decomposed once. It should be noted, however, that when drastic water depression occurs around the drainage system, mesh dependency and numerical instability may not be completely eliminated by the penalized Heaviside function given in Eq. (13), and a strongly converged solution may be hard to obtain. This is especially the case when a complex drainage system is involved and a coarse finite element mesh is used. The main reason is that the definition of the penalized Heaviside function, H_λ (with a requirement to approximate the Heaviside function, H, as the mesh being refined) is so strict that only a very few number of nodes close to the free surface are assigned with penalized weights, thus resulting in numerical jumps at the seepage points on the potential seepage surfaces between successive iterations in locating the free surface.

To overcome this problem, we propose an adaptive procedure through progressively relaxing the definition of the penalized Heaviside function. Redefine the penalized Heaviside function in Eq. (13) as

$$H_\lambda(\phi - z) = \begin{cases} 1 & \text{if } \phi \leqslant z - \zeta\lambda_1 \\ \frac{z + \zeta\lambda_2 - \phi}{\zeta(\lambda_1 + \lambda_2)} & \text{if } z - \zeta\lambda_1 < \phi < z + \zeta\lambda_2 \\ 0 & \text{if } \phi \geqslant z + \zeta\lambda_2 \end{cases} \tag{20}$$

in which a parameter, ζ, is introduced to scale values of parameter λ_1 and λ_2 while keeping the form of Eq. (13) and the definitions of λ_1 and λ_2. The value of ζ is suggested to range from 1 to 10. Initially, ζ is set to 1. As the algorithm proceeds, ζ is incrementally adjusted according to convergence condition and mesh size. The incremental value of ζ can be fixed between 0.5 and 1. Generally, a larger value of ζ is required for strongly non-linear problems with coarse meshes and stronger convergence criteria. One can observe that the introduction of ζ in the suggested range does not significantly influence the behaviour of the penalized Heaviside function, but results in very good numerical convergence. For the challenging numerical examples given in Section 4, it is easy to readily reach the converged solutions with this adaptive procedure, but fails when the original form of the function, Eq. (13), is directly applied.

4. Numerical examples

In this section, we give two challenging numerical examples to demonstrate the effectiveness and robustness of the proposed method.

4.1. A rectangular dam with drainage tunnels

As a demonstrative example, a homogenous rectangular dam with five drainage tunnels and an impermeable base is firstly considered, as shown in Fig. 6. The size of the cross-section of the dam is 10 m in width and 12 m in height. The prescribed water head is 10 m on the upstream surface and 2 m on the downstream surface. Quadrilateral elements of uniform size of $0.2\,\text{m} \times 0.2\,\text{m}$ are used to discretize the domain.

If no drainage tunnels are deployed in the dam, then the following empirical solution is available to locate the free surface [15]:

$$z = (100 - 8x)^{1/2} \tag{21}$$

with $z = 4.47$ m at the seepage point, as plotted by curve 2 in Fig. 6. The corresponding numerical solution is shown by curve 1, which matches well with the empirical solution. The numerical solution, however, predicts a relatively more obvious depression of free surface than the empirical one, with $z = 4.20$ m at the seepage point.

As the drainage tunnels with size of cross-sections of $1\,\text{m} \times 1\,\text{m}$ are deployed, the free surface is drastically depressed, as illustrated by curve 3 in Fig. 6. The three tunnels close to the upstream dam surface play a deciding role
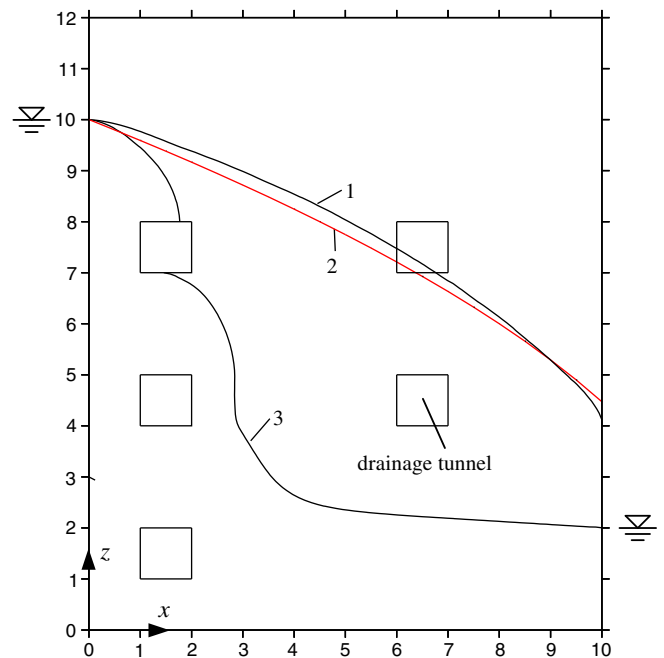

Fig. 6. Locations of the free surfaces in the rectangular dam: (1) numerical solution, no drainage tunnels; (2) empirical solution, no drainage tunnels and (3) numerical solution, with drainage tunnels).

in depressing the free surface, resulting in a loss of effect of the other two in drainage.

4.2. A dam section with drainage galleries and drainage hole array

As a more realistic example of engineering application of the proposed method, we now investigate the effects of a drainage system designed for the roller compacted concrete (RCC) gravity dam of the Guangzhao Hydropower Project on the Beipanjiang River in Guizhou Province, China. The geological conditions of the dam site and the material properties of the RCC gravity dam are simplified in this study, since the main focus is to verify the effectiveness of the proposed method.

Fig. 7 illustrates a typical dam section with a drainage system composed of seven drainage galleries and a drainage hole array. The size of the dam section is 170 m in height and 30 m in width. Other dimensions of the dam and rock foundation of concern are depicted in Fig. 7. The drainage galleries are deployed close to the upstream dam surface and in the rock foundation. For simplicity, a rectangular cross-section is assumed for the galleries, with a cross-sectional size of 2 m × 2 m. Drainage holes are vertically deployed in the dam close to the upstream surface and in the rock foundation immediately behind the grouting curtain. The drainage galleries close to the upstream dam surface are connected by the vertical drainage holes to form a drainage system. The drainage holes are deployed with 5 m in spacing, and the size of the cross-sections of the holes is assumed to be 10 × 10 cm (i.e., 12.73 cm in diameter for circular holes with the same perimeter length). The drainage holes in the rock foundation are 40 m in depth, and the grouting curtain is 2.5 m in thickness and 60 m in depth. An anti-seepage layer is designed on the upstream surface of the dam to reduce the seepage flow, with a thickness of 0.8 m.

Corresponding to an exceptional flood level, the prescribed water head is 168.0 m on the upstream dam surface, and 28.5 m on the downstream dam surface. The bottom and the lateral boundaries in the x- and y-directions of the rock foundation, as well as the lateral boundaries in the y-direction, are assumed to be impermeable. The drainage holes deployed in the rock foundation are prescribed with a water head equal to the floor elevation of the connected drainage gallery. The remaining boundaries, including the galleries and the drainage holes deployed in the dam body, are taken as the potential seepage surfaces. All the materials are assumed to be hydraulically isotropic, and the following values of hydraulic conductivity are taken: $k = 1.62 \times 10^{-6}$ m/d for the anti-seepage layer, $k = 4.09 \times 10^{-6}$ m/d for the concrete dam body, $k = 7.18 \times 10^{-3}$ m/d
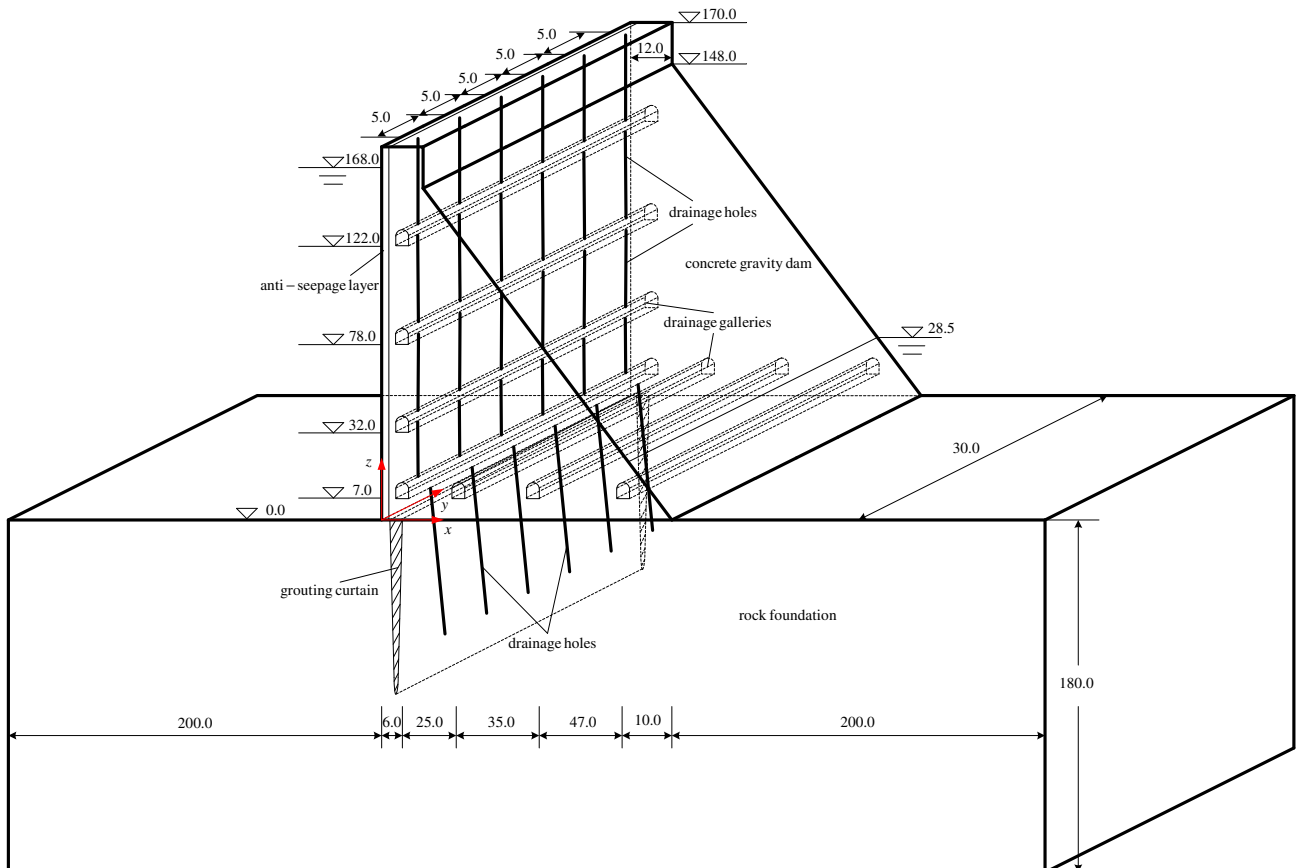

Fig. 7. Illustration of a concrete gravity dam section with drainage hole array and drainage galleries.
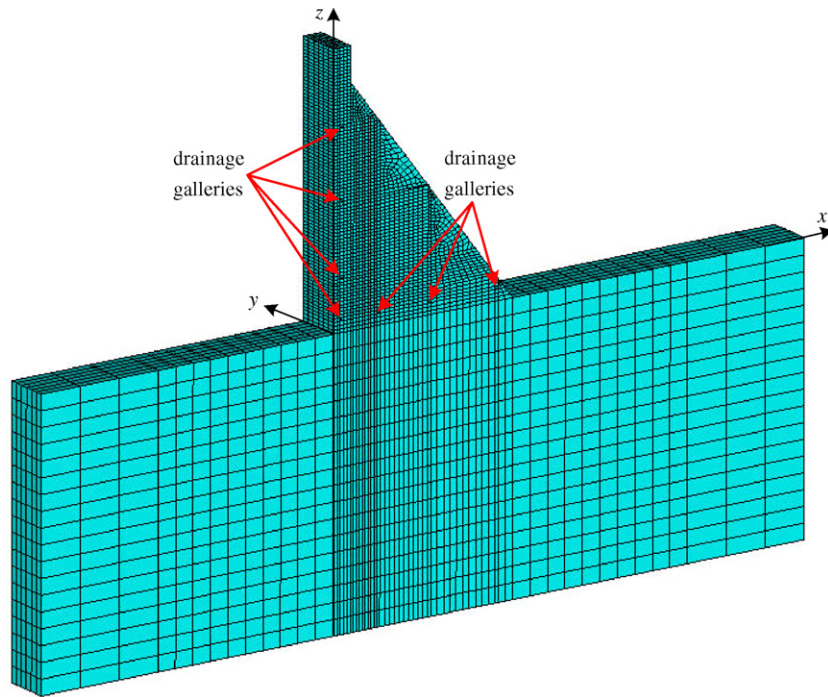
Fig. 8. The element mesh for the dam section. (elements: 19,032; nodes: 23,275).

for the grouting curtain, and $k = 2.30 \times 10^{-2}$ m/d for the rock foundation. A FEM element mesh was generated, as shown in Fig. 8, with 19,032 brick elements and 23,275 nodes. Substructures with three layers of sub-elements in the radial direction (see Fig. 5b) are used to model the drainage holes.

Fig. 9 shows the water head contours at a cross-section parallel to the x-axis and intersecting one set of drainage

holes. Fig. 10 plots the water head contours at the same cross-section under the condition that no drainage holes are installed but the drainage galleries and the grouting curtain are deployed in the same way. A comparison between these two figures demonstrates that the drainage hole array has a dramatic impact on the seepage flow and can sharply depress the free surface, resulting in a remarkable fall of uplift pressure on the dam base, as
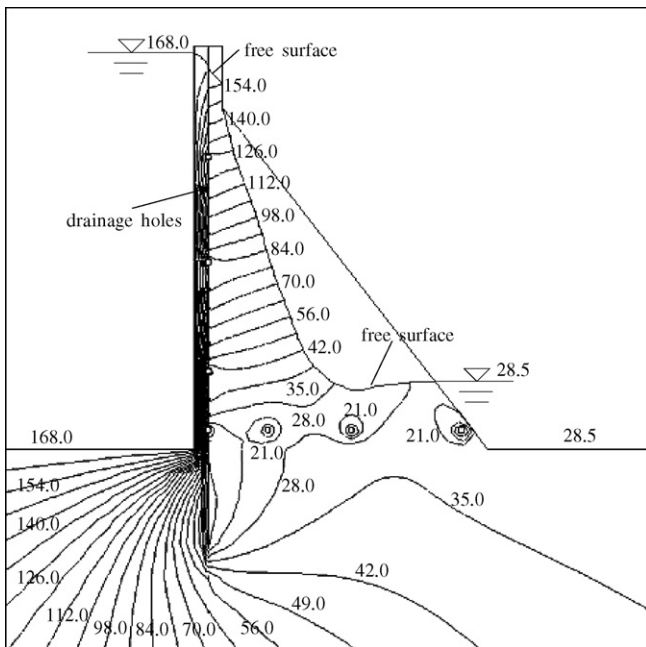

Fig. 9. The water head contours in unit of m at a cross-section parallel to x-axis across one set of drainage holes.
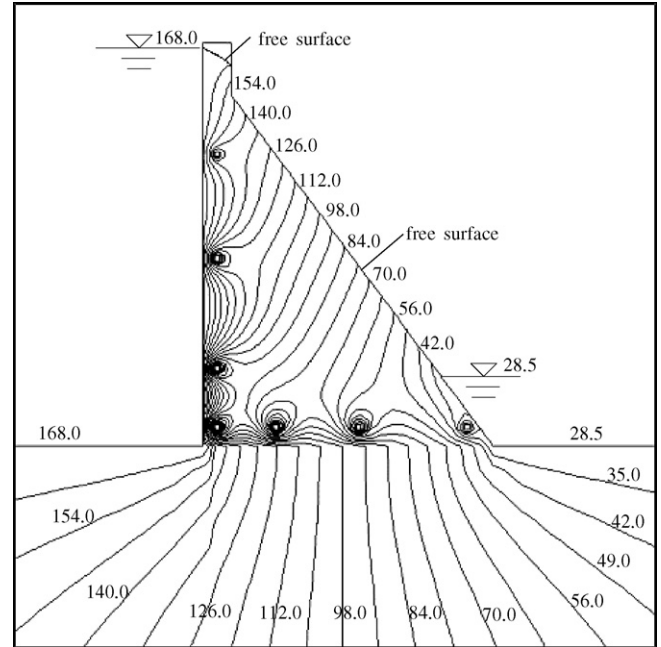

Fig. 10. The water head contours in unit of m at the same cross-section with Fig. 9 under the condition that no drainage holes are installed.

shown in Fig. 11. In addition, it can be inferred from Figs. 9–11 that the drainage galleries with moderate size and large distance have only a local influence on the distribution of the seepage field around, while the drainage hole array with small radius and dense spacing exerts a global
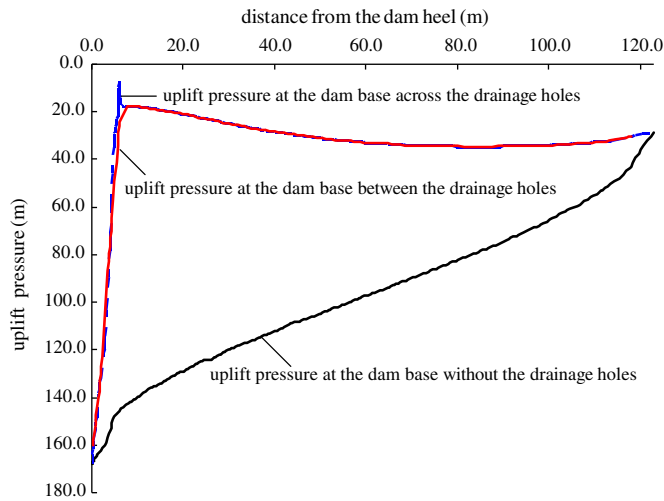

Fig. 11. Comparison of uplift pressure at the dam base with and without deployment of the drainage holes.

effect. This indicates that numerical modeling of drainage holes is indispensable for engineering safety assessment and design optimization.

Fig. 12 shows the water head and the pore water pressure contours at the cross-section parallel to the y-axis and intersecting the drainage hole array. From Fig. 12, one observes that the drainage system composed of the connected drainage hole array and galleries leads to a significant reduction in the pore water pressure around the drainage facilities.

To further validate the effectiveness of the proposed method, a sensitivity analysis is performed to investigate the effects of the deployment pattern of the drainage hole array on the seepage behavior within the dam. First, we maintain the diameter of the drainage holes to be a constant (12.73 cm in this study), but vary the spacing of the holes, s, from 2 to 6 m, with an increment of 1 m. The locations of the free surfaces in the dam with different hole spacing are depicted in Fig. 13, and the flow rates per unit width out of the drainage system composed of the drainage galleries and the drainage hole array are shown in Table 1. One may observe from Fig. 13 that with the decrease of the hole spacing, the free surface in the dam is remarkably depressed and the pore water pressure is effectively reduced, especially for the case that the hole spacing is
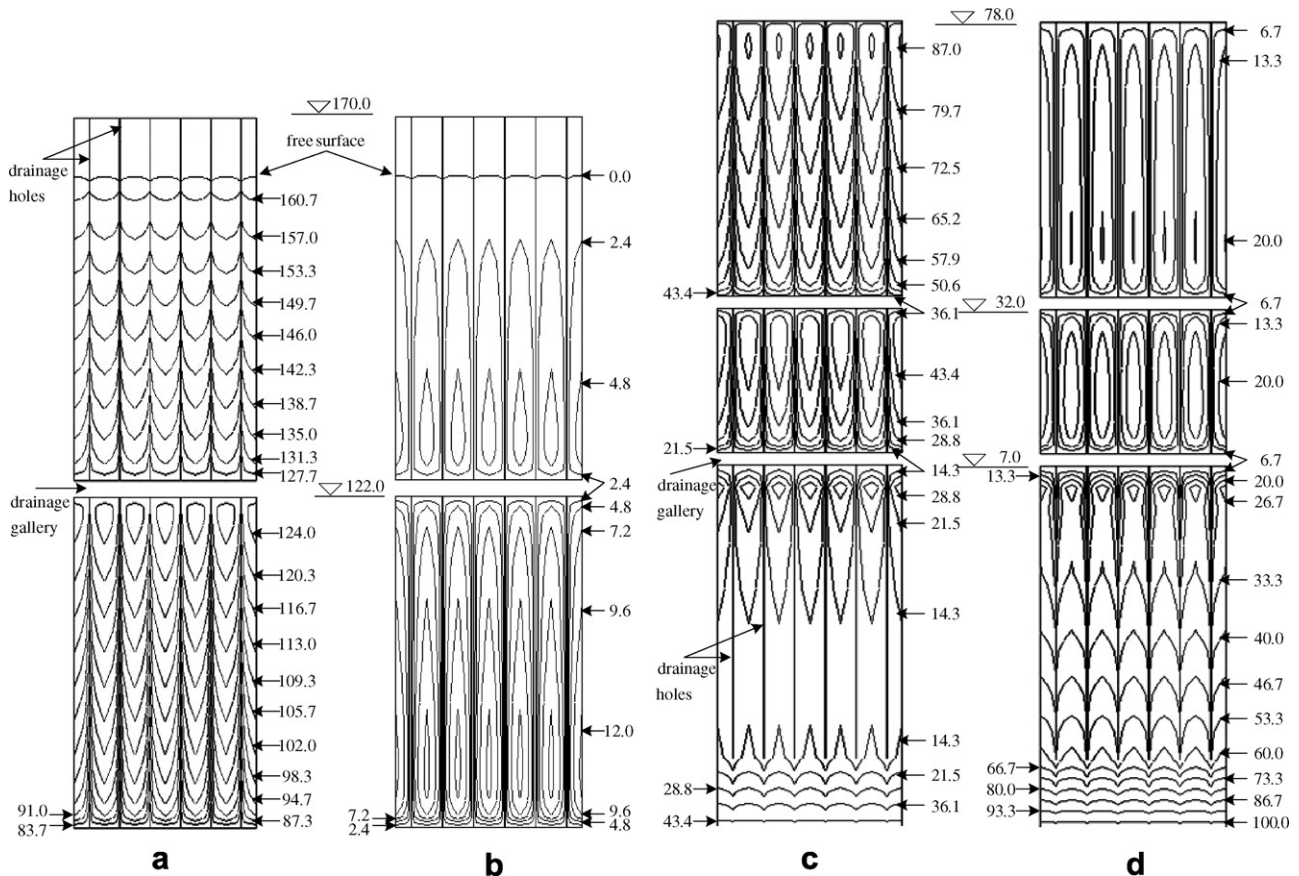

Fig. 12. The water head contours and pore water pressure contours in unit of m at the cross section parallel to y-axis across the drainage hole array: (a) water head contours for $z \geqslant 80$ m; (b) pressure contours for $z \geqslant 80$ m; (c) water head contours for $z \leqslant 78$ m and (d) pressure contours for $z \leqslant 78$ m).
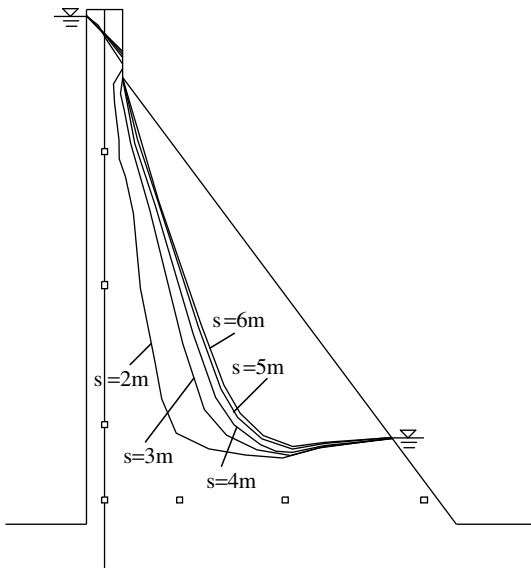
Fig. 13. Locations of the free surfaces at a cross-section parallel to *x*-axis across one set of drainage holes as the hole spacing, *s*, varies from 2 to 6 m.

Table 1
The drainage flow rate per unit width out of the drainage system with different hole spacing

Hole spacing (m)	2	3	4	5	6
Flow rate per unit width (m³/d)	6.937	6.970	6.946	6.918	6.892

smaller than 4 m. It can be further observed from Table 1 that the variation of the hole spacing in the specified range does not significantly affect the flow rate out of the drainage system. This is because that as the hole spacing decreases, the pore water pressure surrounding the drainage system also reduces. As a result, the increase in drainage flow rate due to increase of the number of the drainage holes is basically counteracted by the decrease in drainage flow rate due to reduction of the pore water pressure. This does not mean, however, that the drainage flow rate plays a secondary role in the optimization design of the drainage system. As the permeability of the dam and the rock foundation or the water head prescribed on the upstream and downstream surfaces changes, change in the flow rate out of the drainage system will inevitably occur.

Second, we maintain the spacing of the drainage holes to be a constant (5 m is this study), but vary the diameter of the holes, *d*, from 5 to 20 cm, with an increment of 5 cm. The locations of the free surfaces in the dam corresponding to different hole diameter are illustrated in Fig. 14, and the flow rates out of the drainage system are listed in Table 2. One may observe that with the increase of the hole diameter, the free surface is slightly depressed and the drainage

Table 2
The drainage flow rate per unit width out of the drainage system with different hole diameter

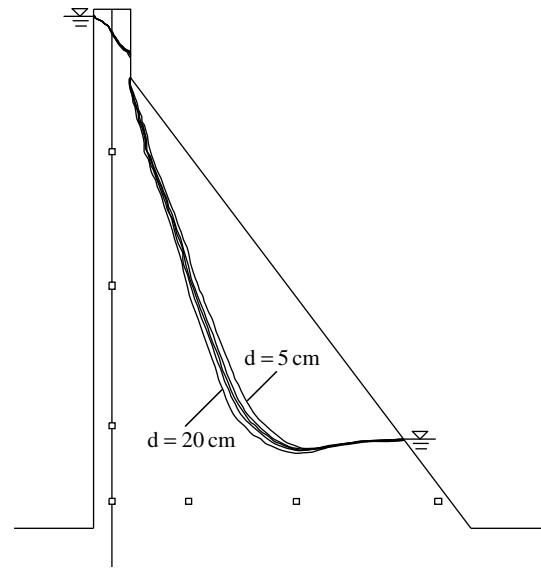| Hole diameter (cm)	5	10	12.73	15	20
Flow rate per unit width (m³/d)	6.863	6.899	6.918	6.933	6.966

Fig. 14. Locations of the free surfaces at a cross-section parallel to *x*-axis across one set of drainage holes as the hole diameter, *d*, varies from 5 to 20 cm.

flow rate per unit width is slightly reduced, but both of the changes are not significant. This indicates that the commonly-used hole diameter between 5 and 15 cm is suitable in engineering.

The numerical results achieved in this challenging example demonstrate, on the one hand the effectiveness and robustness of the proposed method, and on the other hand the importance of predictive modeling of the drainage system for performance and safety assessments and optimization of designs. Other methods, such as the semi-analytical method [5] or the composite element method [7], may be valid for modeling the drainage holes in rock foundation with prescribed water pressures, but very likely fail to model a complex drainage system due to their simplified characterization of the boundary conditions of the drainage facilities.

5. Conclusions

Seepage problems with complex drainage systems are commonly faced in dam engineering, slope engineering and underground engineering, and are typically non-linear. Combined with the substructure technique and the variational inequality formulation of Signorini's type, a numerical solution with the FE method is suggested in this study. The effectiveness and robustness of the proposed method are validated by two challenging numerical examples. The main contributions in this study are summarized below:

(1) The boundary conditions of the drainage system composed of drainage holes, drainage tunnels (galleries), and drainage wells are characterized by using a water head condition, the complementary condition of Signorini's type, or the combined boundary condi-

tion of both. For drainage facilities satisfying the combined boundary conditions, an iterative procedure is suggested to determine the water head of the free surface that has to be prescribed by ensuring flow equilibrium.

(2) A substructure technique is introduced to model the drainage hole array with small radius and dense spacing. As a result, the difficulties in mesh-generating and equation-solving tasks are avoided.

(3) Combined with an adaptive procedure for progressively relaxing the penalized Heaviside function, the variational inequality formulation of Signorini's type is used to determine the seepage points and to locate the seepage free surfaces. With this method, not only the singularity at the seepage points and the resultant mesh dependency are completely eliminated, but also the numerical stability and robustness of the algorithm are satisfactorily achieved.

(4) The focus of this paper is the effects of drainage systems in different engineering practices. The total assessment of performance and safety of such engineering facilities, such as those considering coupled hydro-mechanical effects on seepage behaviour and safety, is outside the scope of the current investigation.

Acknowledgements

References

[1] Chen SH, Wang WM, She CX, Xu MY. Unconfined seepage analysis of discontinuous rock slope. J Hydrodyn, Ser B 2000;12(3):75–86.

[2] Wang L, Liu Z, Zhang YT. Analysis of seepage field near a drainage holes curtain. Chin J Hydraulic Eng 1992;12(4):15–20.

[3] Zhu YM, Zhang LJ. Solution to seepage field problem with the technique of improved drainage substructure. Chin J Geotech Eng 1997;19(2):69–76.

[4] Fipps G, Skaggs RW, Nieber JL. Drains as a boundary condition in finite elements. Water Resour Res 1986;22(11):689–707.

[5] Zhan ML, Su BY. New method of simulating concentrated drain holes in seepage control analysis. J Hydrodyn, Ser B 1999;11(3):27–35.

[6] Wang EZ, Wang HT, Deng XD. A numerical method for simulating single drainage hole in rock masses. Chin J Rock Mech Eng 2001;20(3):346–9.

[7] Chen SH, Xu Q, Hu J. Composite element method for seepage analysis of geotechnical structures with drainage hole array. J Hydrodyn, Ser B 2004;16(3):260–6.

[8] Desai CS, Li GC. A residual flow procedure and application for free surface in porous media. Adv Water Resour 1983;6(1):27–35.

[9] Zhang YT, Chen P, Wang L. Initial flow method for seepage analysis with free surface. Chin J Hydraulic Eng 1988;8(1):18–26.

[10] Bathe KJ, Khoshgoftaar MR. Finite element free surface seepage analysis without mesh iteration. Int J Numer Anal Methods Geomech 1979;3(1):13–22.

[11] Zheng H, Liu DF, Lee CF, Tham LG. A new formulation of Signorini's type for seepage problems with free surfaces. Int J Numer Methods Eng 2005;64:1–16.

[12] Brezis H, Kinderlehrer D, Stampacchia G. Sur une nouvelle formulation due probleme de l' ecoulement a travers une digue. Comptes Rendus de l'Academie des Sciences Paris Series A 1978;287:711–4.

[13] Zheng TS, Li L, Xu QY. An iterative method for the discrete problems of a class of elliptical variational inequalities. Appl Math Mech 1995;16(4):351–8.

[14] Meurant G. A review on the inverse of symmetric tridiagonal and block tridiagonal matrices. SIAM J Matrix Anal Appl 1992;13(2):707–28.

[15] Zhou CB, Xiong WL, Liang YG. A new method for unconfined seepage field. J Hydrodyn, Ser A 1996;11(5):528–34.